

The Photoconductor Array Camera & Spectrometer (PACS) for the Far Infrared and Submillimetre Telescope (FIRST)

A. Poglitsch^a, C. Waelkens^b, and N. Geis^a

^aMax-Planck-Institut f. Extraterrestrische Physik, Postfach 1603, D-85740 Garching, Germany

^bKatholieke Universiteit Leuven, Celestijnenlaan 200B, B-3001 Leuven, Belgium

ABSTRACT

The Photoconductor Array Camera & Spectrometer (PACS) is one of the three science instruments for ESA's Far Infra-Red and Submillimetre Telescope (FIRST). It employs two 16×25 pixels Ge:Ga photoconductor arrays (stressed/unstressed) to perform imaging photometry and imaging line spectroscopy in the $60 - 210\mu\text{m}$ wavelength band. In photometry mode, it will simultaneously image two bands, $60 - 90$ or $90 - 130\mu\text{m}$ and $130 - 210\mu\text{m}$, over fields of view of $\sim 1' \times 1.5'$ and $\sim 2' \times 3'$, respectively, with full beam sampling in each band. In spectroscopy mode, it will image a field of $\sim 50'' \times 50''$, resolved into 5×5 pixels, with an instantaneous spectral coverage of $\sim 1500\text{km/s}$ and a spectral resolution of $\sim 175\text{km/s}$. In both modes background-noise limited performance is expected, with sensitivities (5σ in 1h) of $4 - 6$ mJy or $2 - 8 \times 10^{-18}\text{W/m}^2$, respectively.

Keywords: Infrared, submillimeter, photoconductor, array, imaging, photometer, spectrometer

1. INTRODUCTION

The Far Infra-Red and Submillimetre Telescope (FIRST) is the fourth cornerstone mission of ESA's Horizon 2000 program. It is defined as a multi-user "observatory type" mission with the goal to open up the wavelength range $\leq 80 - 600\mu\text{m}$ to photometry and spectroscopy with unprecedented sensitivity and spatial resolution, unobscured by the Earth's atmosphere.

The scientific topics of the mission include the formation and evolution of galaxies in the early Universe, the question what powers luminous galaxies, the search for protostars in our own Galaxy, a better understanding of how stars form out of the interstellar medium, and the evolution of planetary systems including the Solar System.

Many of the involved processes are known to emit most of their luminosity in the far-infrared and sub-millimeter band, both as continuum radiation from dust and as spectral line features. Within the complement of three instruments selected to form the science payload,¹⁻⁸ the shortest wavelength band, $60 - 210\mu\text{m}$, will be covered by the Photoconductor Array Camera & Spectrometer (PACS), which will provide both photometric and spectroscopic observing modes suited to address the key scientific topics of the FIRST mission.

In this paper we describe the design of PACS which has been proposed to ESA by a consortium of European research institutions with the goal to develop and operate the instrument and the associated Instrument Control Centre. The present concept is the outcome of an optimization process toward best observing efficiency regarding the key science of FIRST and toward simplicity of operation, and in the context of competing/complementary missions like SOFIA or SIRTf.

2. INSTRUMENT REQUIREMENTS

The advantage of FIRST in its core wavelength range – compared to missions like SIRTf and SOFIA or ground based facilities – is its unique combination of angular resolution and sensitivity which enables the scientific program foreseen with FIRST. The key scientific topics to be addressed with FIRST require from PACS the provision of diffraction/telescope-limited, broad-band photometric imaging, and of medium-resolution spectroscopic capabilities, at wavelengths from $\sim 60\mu\text{m}$ to $> 200\mu\text{m}$. The lower wavelength limit is mainly determined by the surface quality of the FIRST telescope; at shorter wavelengths FIRST will not be able to maintain its advantage over SIRTf in terms of angular resolution.

E-mail: alpog@mpe.mpg.de

2.1. Photometer Requirements

Photometric color diagnostics requires spectral bands with a relative bandwidth $\Delta\lambda/\lambda \sim 2$. In coordination with SPIRE, the PACS photometric bands have been defined as $60 - 90\mu\text{m}$, $90 - 130\mu\text{m}$, and $130 - 210\mu\text{m}$.

A major fraction of the FIRST observing time will go to deep and/or large scale photometric surveys. For these, mapping efficiency is of the highest priority. Mapping efficiency is determined by both, the instantaneous field of view of the instrument (number of pixels) and the sensitivity per pixel. How the two parameters enter into a measure of the mapping efficiency greatly depends on the mapped objects. A main discriminator is the confusion limit (source separation \sim beam size): If confusion is reached after a reasonably short integration time, then sensitivity per detector can be traded for number of pixels. In the opposite case, the sensitivity per pixel is the more important parameter. Within the PACS bands, the confusion limit in selected fields is expected as low as a few mJy (5σ), and detector sensitivity (if a trade-off turned out necessary) has to get higher priority than number of pixels. Thus, the PACS instrument has to be designed around the largest possible detector arrays affordable without a compromise in sensitivity, i.e., with the highest possible system detective quantum efficiency and telescope background limited noise performance.

Simultaneous observation of – preferably all – photometric bands is also suggested by the need to maximize observing efficiency, and a by-product when detector technology requires different detectors to cover the full PACS wavelength band with optimum sensitivity.

Extraction of very faint sources from the very bright telescope background has to be ensured, by a combination of intrinsic photometric stability and ways to precisely flat-field the system responsivity on as short a timescale as necessary, as well as by spatial modulation techniques (chopping/nodding, on-the-fly mapping).

2.2. Spectrometer Requirements

The key spectroscopic observations ask for the detection of weak spectral lines with medium resolution ($R \sim 1500$). The sources to be observed may have precisely known positions or, in the case of follow-up observations to the photometric surveys, only within the absolute position error of the FIRST satellite. In any case, the intrinsic uncertainty in the satellite pointing should not compromise the measurement, neither in sensitivity nor in spatial resolution. Subtraction of the high telescope background must be accomplished.

Sensitivity is the most important parameter for optimisation; with background-limited performance the best sensitivity is obtained if the spectrometer fulfills the following conditions: The detection bandwidth must not be greater than the resolution bandwidth, which should be matched to the line width of the source, and the line flux from the source must be detected with the highest possible efficiency in terms of system transmission, spatial and spectral multiplexing.

Wavelength calibration accurate to a fraction of the resolution bandwidth must be ensured for all observations. Intensity calibration and removal of modulations in the spectral response (defringing) must be provided for.

3. INSTRUMENT CONCEPT

The instrument concept has been developed based on the requirements stated above on the one hand, and within the boundary conditions set by the FIRST satellite and the available detector technology on the other hand. Use of the thus defined “phase space” has been mainly defined by the resources which are at the disposal of the PACS consortium.

The instrument will offer two basic modes in the wavelength band $60 - 210\mu\text{m}$:

- Imaging dual-band photometry ($60 - 90$ or $90 - 130\mu\text{m}$ and $130 - 210\mu\text{m}$) with fields of view of $\sim 1' \times 1.5'$ and $\sim 2' \times 3'$, respectively, with full sampling of the telescope point spread function (diffraction/wavefront error limited)
- Integral-field line spectroscopy between $57\mu\text{m}$ and $210\mu\text{m}$ with a resolution of $\sim 175\text{km/s}$ and an instantaneous coverage of $\sim 1500\text{km/s}$, over a field of view of $\sim 1' \times 1'$

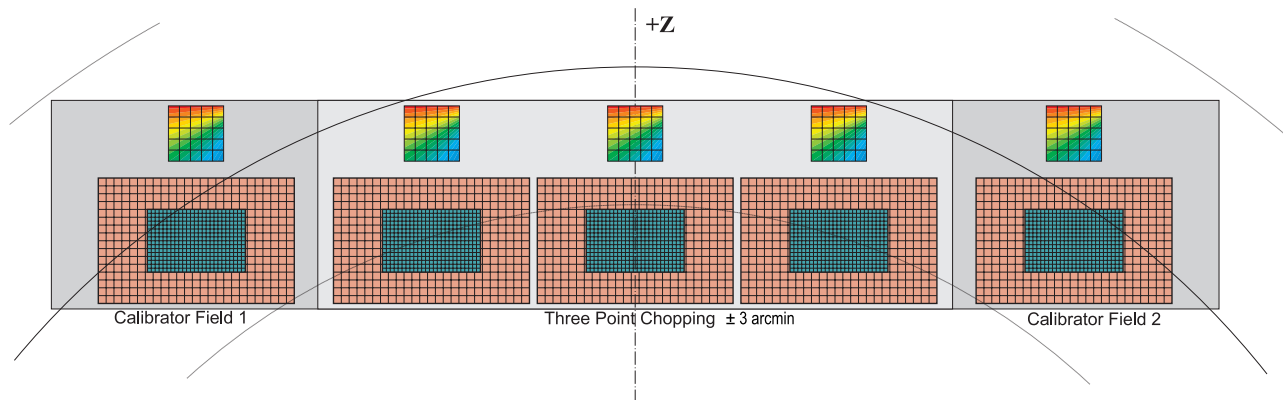


Figure 1. *PACS focal plane usage. Long-wavelength (red) and short-wavelength (blue) photometry bands cover concentric fields of view. The spectrometer field of view is offset in the +z direction. Chopping is done along the y axis (left-right in this view) and also allows observation of the internal calibrators on both sides of the used area in the telescope focal plane. The circle arcs are centered on the FIRSA telescope axis*

Both modes will allow spatially chopped observations by means of an instrument-internal chopper mirror with variable throw; this chopper also is used to alternatively switch two calibration sources into the field of view.

The focal plane sharing of the instrument channels is shown in Fig. 1.

The photometric bands, which can be observed simultaneously, are concentric, while the field of view of the spectrometer is offset from the photometer field of view. Since photometry and spectroscopy are mutually exclusive this has no effect on the observing efficiency.

The focal plane unit provides these capabilities through four functional units:

- common input optics with the chopper, calibration sources and a focal plane splitter
- a photometer optical train with a dichroic beam splitter and separate re-imaging optics for the short-wavelength bands (60 – 90 / 90 – 130 μm) and the long-wavelength band (130 – 210 μm), respectively
- a spectrometer optical train with an image slicer unit for integral field spectroscopy, an anamorphic collimator, a diffraction grating in Littrow mount with associated actuator and position readout, and a dichroic beam splitter for separation of diffraction orders
- 2 detector arrays with attached cryogenic readout electronics (CRE) and flip mirror assemblies for switching between photometry and spectroscopy

A detailed description of the FPU design is given in a separate paper.⁹

3.1. Photoconductor Arrays

The 25 \times 16 pixels Ge:Ga photoconductor arrays are extensions of the 16 \times 16 pixels stressed Ge:Ga photoconductor array which has been demonstrated by the ESA-supported FIRSA study.^{10,11} The stressed 25 \times 16 array for the long-wavelength band differs from the demonstrator by a more sophisticated stressing mechanism which ensures a homogeneous stress within each pixel along the stack, and by simply employing a larger number of these 16-element linear arrays.¹² The second – “unstressed” – array with a 40% improved short-wavelength responsivity (Fig. 2) is almost identical to the long-wavelength array, except for the mechanical stress on the pixels which will be reduced to about 10% of the level needed for the long-wavelength response. Details of the design of both arrays are described in a separate article.¹³

A computer rendering of a design study of the array is shown in Fig. 2. The light cones in front of the actual detector block provide for area-filling light collection in the focal plane and feed the light into the individual integrating

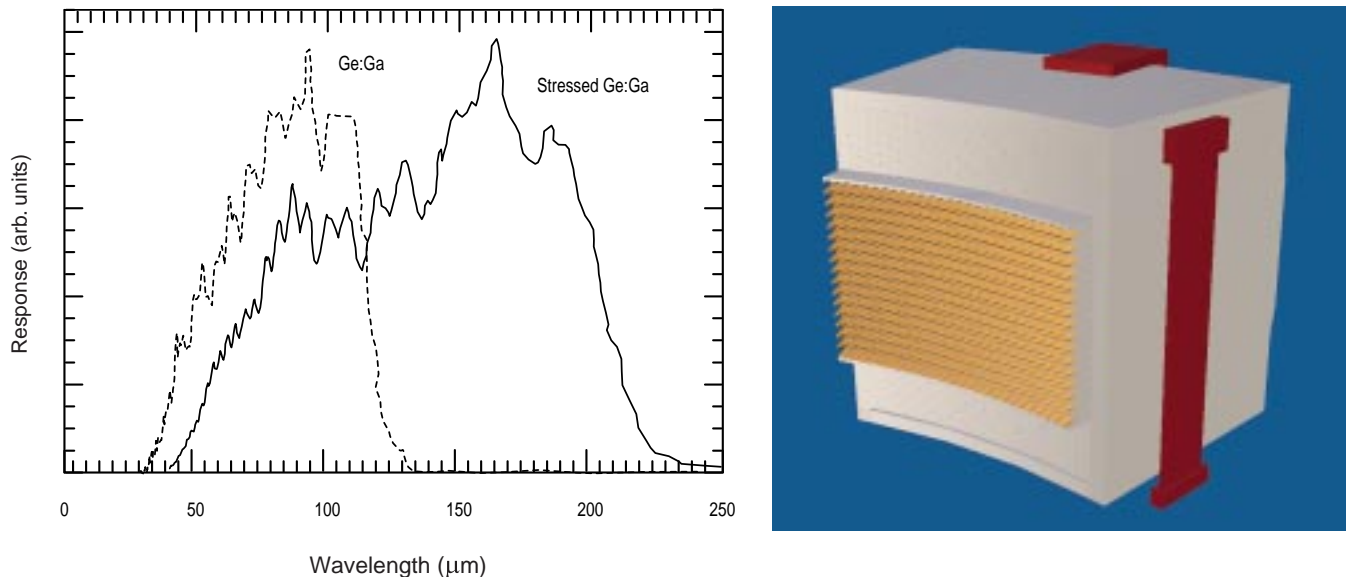


Figure 2. *Left: relative spectral response of stressed (solid trace) and unstressed (dashed trace) Ge:Ga. Right: solid model of the 16×25 stressed Ge:Ga photoconductor array for PACS.*

cavities around each individual, mechanically stressed pixel. The light cones also act as a very efficient means of straylight suppression because their solid angle of acceptance is matched to the re-imaging optics such that out-of-beam light is rejected. The detector material also defines the wavelength range of the instrument which, for a combination of stressed and unstressed Ge:Ga, can be $\sim 50 - 210 \mu\text{m}$.

Each linear module of 16 detectors is read out by a cryogenic amplifier/multiplexer circuit in CMOS technology.¹⁴ The readout electronics is integrated into the detector modules. The high telescope background requires a rapid readout (1/64 s) of each pixel which leads to a raw data rate substantially above the maximum rate allowed by the FIRST on-board data handling system. A combination of (“lossy”) data reduction and lossless data compression^{15,16} is carried out by a dedicated Signal Processing Unit within the PACS warm electronics.

3.2. Entrance Optics, Chopper and Calibrators

The entrance optics fulfills the following tasks: It creates an image of the telescope secondary mirror (the entrance pupil of the telescope) on the instrument chopper; this allows spatial chopping with as little as possible modulation in the background received by the instrument. It also provides for an intermediate pupil position where the Lyot stop and the first blocking filter, common to all instrument channels, can be positioned, and it allows the chopper - through two field mirrors adjacent to the used field of view in the telescope focal surface - to switch between a (chopped) field of view on the sky and two calibration sources (see also Fig. 1).

The chopped image is then re-imaged onto an intermediate focus where a fixed field mirror splits off the light into the spectroscopy channel. The remaining part of the field of view passes into the photometry channels. A “footprint” of the focal-plane splitter is shown in Fig. 3.

The calibration sources (not shown in Fig. 4) are placed at the entrance to the instrument to have the same light path for observation and internal calibration. This is essential for removing baseline ripples as best as possible, a serious task with a warm telescope and the associated high thermal background. To eliminate non-linearity or memory problems with the detector/readout system, the calibrator sources will be gray-body sources providing FIR radiation loads slightly above or below the telescope background, respectively. They also mimic the illumination of the telescope.

The chopper provides a maximum throw of $6'$ on the sky; this allows effective three-point chopping over the full extent of the long-waveband field of view. The chopper¹⁷ is capable of following arbitrary waveforms with a resolution of $1''$ and delivers a duty-cycle of 80% at a chop frequency of 8 Hz.

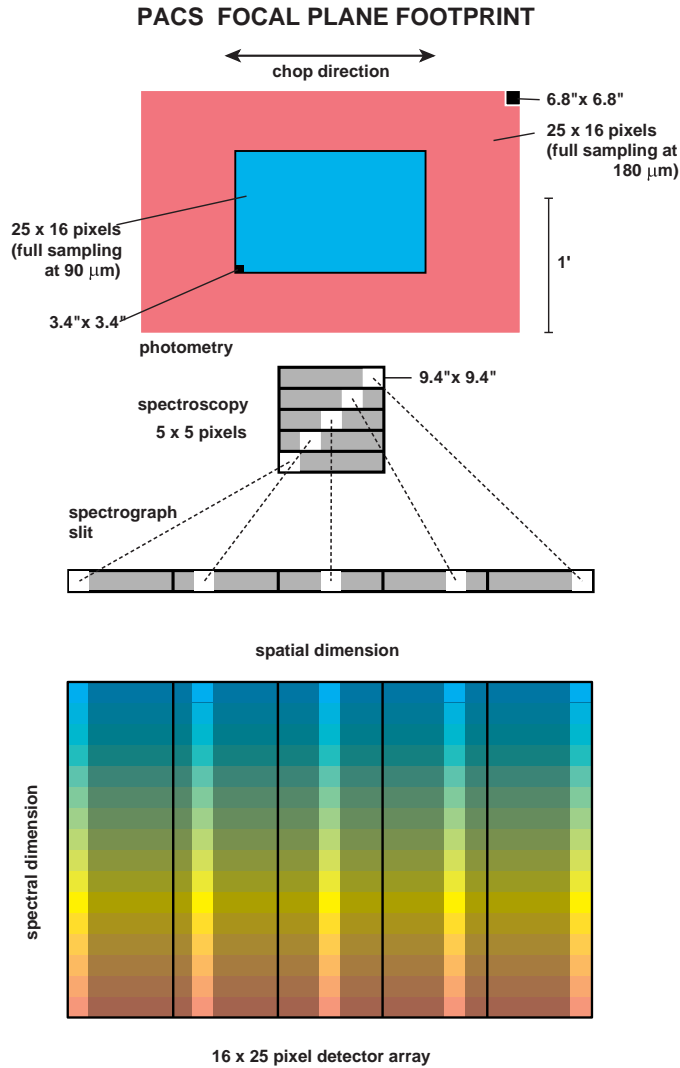


Figure 3. Focal plane footprint. A fixed mirror is used to split the focal plane into the photometry and spectroscopy channels of the instrument. In the photometry section, the two wavelength bands are simultaneously imaged with different magnification to reach full beam sampling in both bands. In the spectroscopy section, an optical image slicer re-arranges the 2-dimensional field along the entrance slit of the grating spectrograph such that, for all spatial elements in the field, spectra are observed simultaneously.

3.3. Imaging Photometer

After the intermediate focus provided by the entrance optics, the light is split into the long-wavelength and short-wavelength channels by a dichroic beamsplitter with a transition wavelength of $130\mu\text{m}$ and re-imaged with different magnification onto the respective detector array (stressed/unstressed).

The 25×16 pixels in each array are used to image a field of view of $\sim 1.5' \times 1'$ in the short-wavelength bands, providing full beam sampling at $90\mu\text{m}$, and $\sim 3' \times 2'$ in the long-wavelength band, with full sampling at $180\mu\text{m}$.

The photometry mode provides simultaneous coverage of two wavelength bands with the two detector arrays of the instrument: The long-wavelength band ($130 - 210\mu\text{m}$) can be combined with either one of the two bands of the short-wavelength channel, $60 - 90\mu\text{m}$ or $90 - 130\mu\text{m}$. The two short-wavelength bands are selected by two filters with an exchange mechanism. All filters are implemented as multi-mesh interference filters (QMW, London).

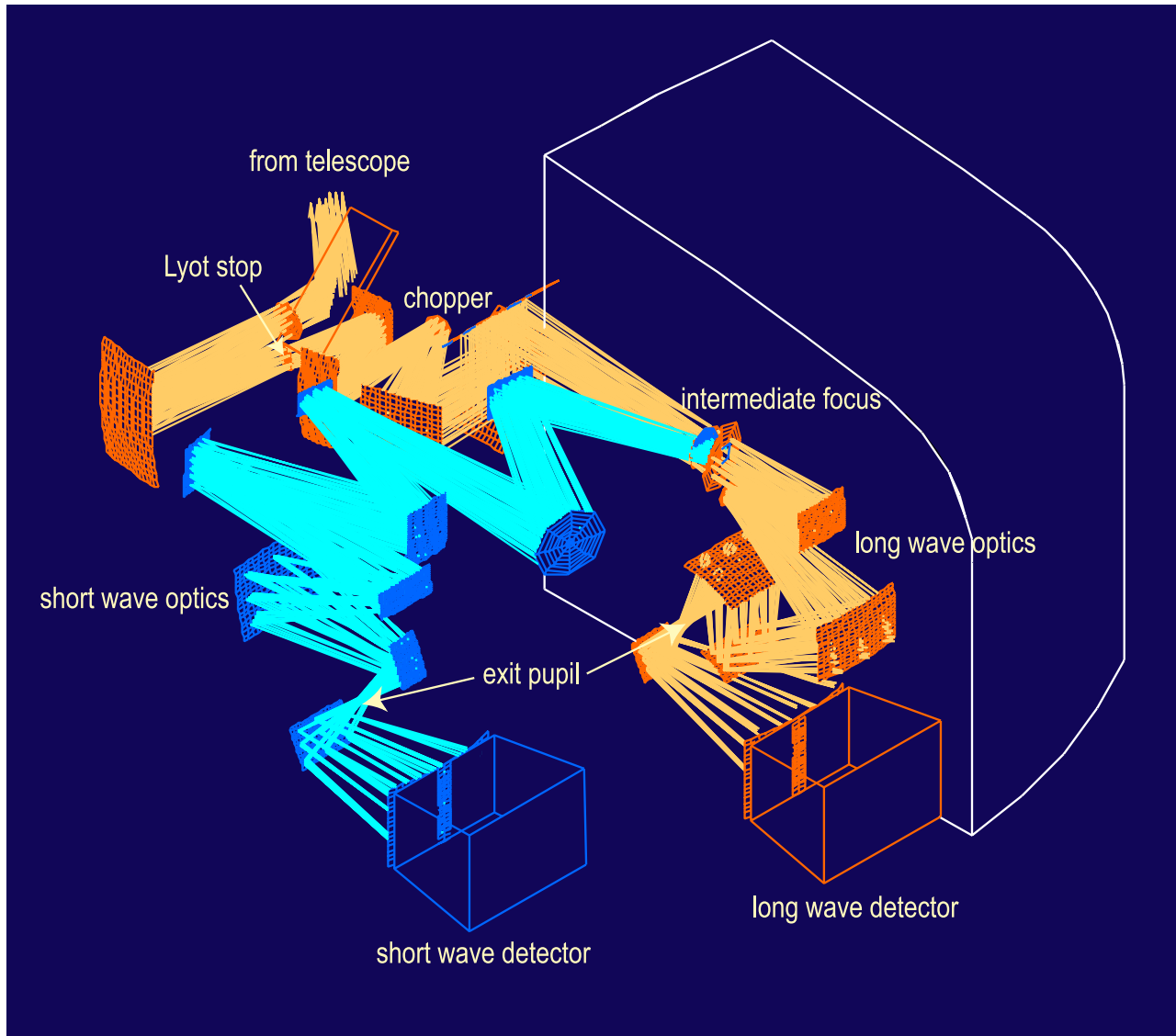


Figure 4. *PACS optics: common entrance optics and the two photometer trains.*

The re-imaging optics also creates exit pupils at a distance from the detector arrays which is matched to the feed optics of the arrays and which allows efficient baffling by the detector compartments.

3.4. The Integral-Field Spectrometer

The spectrometer (Fig. 5) covers the wavelength range from $57\mu\text{m}$ to $210\mu\text{m}$. It provides a resolving power of $1000 - 2000$ ($\Delta v = 150 - 300\text{km/s}$) with an instantaneous coverage of $\sim 1500\text{km/s}$ and simultaneous imaging of a $\sim 50'' \times 50''$ field of view, resolved into 5×5 pixels. An image slicer employing reflective optics is used to re-arrange the 2-dimensional field of view along a 1×25 pixels entrance slit for a grating spectrometer, as schematically shown in Fig. 3.

The integral-field concept has been selected because simultaneous spectral and spatial multiplexing allows the most efficient detection of weak individual spectral lines with sufficient baseline coverage and high tolerance to pointing errors without compromising spatial resolution, as well as for spectral line mapping of extended sources regardless of their intrinsic velocity structure.

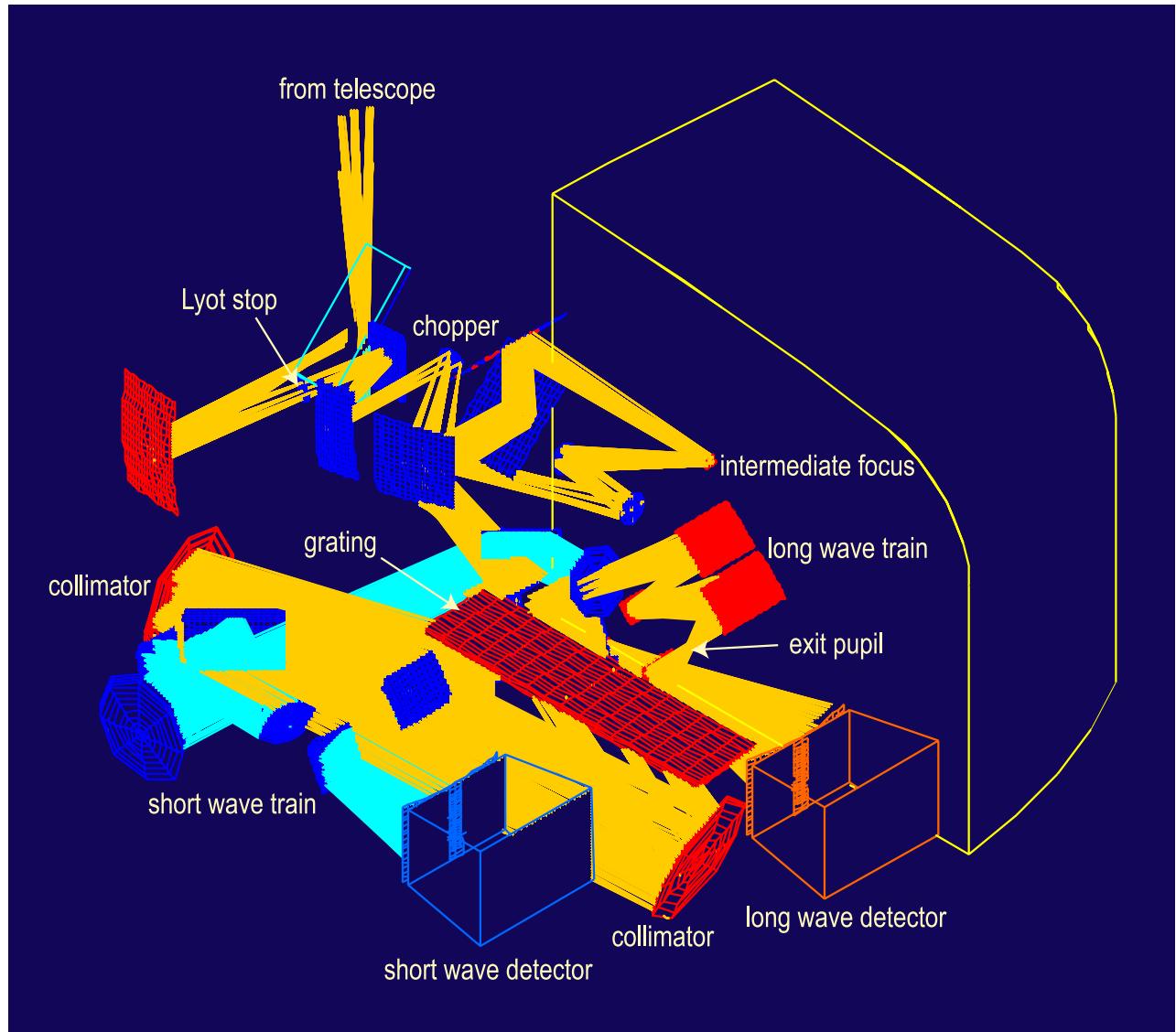


Figure 5. *PACS optics: common entrance optics and the two spectrometer trains.*

The Littrow-mounted grating with a length of $\sim 30\text{cm}$ is operated in 1st, 2nd or 3rd order, respectively, to cover the full wavelength range. The 1st order covers the range $105 - 210\mu\text{m}$, the 2nd order $72 - 105\mu\text{m}$, and the 3rd order $57 - 72\mu\text{m}$. Anamorphic collimating optics expands the beam to an elliptical cross section to illuminate the grating over a length required to reach the desired spectral resolution. The grating is actuated by a cryogenic motor¹⁸ with a resolution of a few arcsec which allows spectral scanning/stepping for improved spectral flatfielding and for coverage of extended wavelength ranges.

The light from the 1st diffraction order vs. light from the other two orders is separated by a dichroic beam splitter and passed on into two optical trains feeding the respective detector array (stressed/unstressed) for the wavelength ranges $105 - 210\mu\text{m}$ and $57 - 105\mu\text{m}$. In each path, anamorphic re-imaging optics is employed to independently match the spatial and spectral resolution of the system to the square pixels of the detector arrays. The filter exchange mechanism in the short-wavelength path selects the 2nd or 3rd grating order.

4. SYSTEM PERFORMANCE

Based on the present knowledge of the components of PACS and of the FIRST satellite, the performance of the entire system can be estimated in terms of what the observer is concerned with, i.e., an assessment of what kind of observations will be feasible with FIRST/PACS, and how much observing time they will require.

The system sensitivity of the instrument at the telescope depends mainly on the optical efficiency, i.e. the fraction of light from an astronomical source arriving at the telescope that actually reaches the detector, and on the thermal background radiation from the telescope or from within the instrument as long as the fluctuations of the background constitute the dominant noise source. As will be shown below, background-noise limited performance can be reached in both spectroscopy and photometry modes with state-of-the-art photoconductors.

4.1. FIRST Telescope

Ideally, the telescope would be diffraction limited over the full PACS wavelength range. The present telescope design allows a wavefront error of $6\mu\text{m}$ (r.m.s.). The type of error is not known; we have assumed spherical aberration for the analysis. The main effect on the point spread function (PSF) is a transfer of power from the central peak to larger radii while the width of the central peak is not affected much. The power concentrated in the central peak (delimited by the first zero of the ideal telescope PSF) as a function of wavelength enters into the sensitivity calculation as “telescope efficiency” because we assume that - for weak/confused sources - only the power in the central peak will be detected.

4.2. Chopper

Errors/jitter in the chopper throw would spread out the power from the central peak. The chopper specification requires an accuracy of $1''$ on the sky; with beam widths of $> 6''$ (FWHM) the effect of pointing errors introduced by the chopper is negligible. However, with the high background of the FIRST telescope, any gradient in this background will lead to noise due to chopping jitter. With the present thermal model of the telescope, this chopping noise will still be tolerable compared to the background noise. The duty cycle of the PACS chopper is $> 80\%$, i.e., $> 80\%$ of the observing time is used for integration.

4.3. Mirrors and Filters

The PACS optics employs a large number of mirrors in each instrument channel. Therefore, the loss per mirror is an important number for the overall transmission of the system. Losses occur by absorption in the mirror material, by scattering at the mirror surface, and by diffraction losses due to the finite mirror sizes. Without diffraction which can be treated separately, the combined scattering/absorption losses per mirror surface can be less than 1% at FIR wavelengths, but measurements also show that they vary with material and surface treatment, and we assume a value of 1%. From the number of reflections a loss of 26% for the spectrometer channels and of 15% for the photometer channels is derived.

The transmission of the filter chain in each of the instrument channels will be $> 40\%$, the value we assume to model the system.

4.4. Diffraction Losses

The most serious diffraction effects are expected in the image slicer. Therefore, an end-to-end diffraction analysis from the telescope focus through the spectrometer train to the detector array has been carried out with the physical optics package GLAD4.5 and, for the image slicer, been confirmed by an exact, vectorial diffraction calculation.¹⁹ From this diffraction analysis we obtained a total loss of 15%; as an upper limit we assume the same number for the short-wavelength channel. The diffraction within the photometer channels has not been calculated, yet. For a preliminary estimate we assume that the diffraction effects must be much smaller than in the spectrometer because in the photometer all mirrors are substantially oversized. Thus, the diffraction loss is within the error margins of the absorption/scattering losses of the mirror system and can be neglected. Diffraction in the shared entrance optics may require an undersized Lyot stop with a further loss of $\sim 10\%$ which has been included in the sensitivity calculation.

4.5. Grating Efficiency

The grating profile has been analyzed with a full electromagnetic code (PCGrate) and optimized for uniform efficiency over the three orders used in PACS.¹⁹ A representative mean value of 65% is adopted for this analysis.

4.6. Detectors

The projected (dark) detector NEP is $\leq 5 \times 10^{-18} \text{ W Hz}^{-1/2}$, a value which will ensure background-limited performance and which has already been reached with similar designs in a balloon-borne experiment.²⁰ Detective quantum efficiencies of $\sim 30\%$ are feasible with careful cavity design.²¹

4.7. Image Quality and Beam Sampling

The photometer optics delivers diffraction-limited image quality. We therefore assume that the instrument optics will only contribute in a negligible way to the dilution of the central peak of the telescope PSF.

The concept of approximately full beam sampling with our (filled) array will distribute the flux of a point source over several pixels. An equivalent dilution applies to the background received by the pixel. To recover the total flux (in the central peak of the PSF) several pixels have to be co-added. For the calculation of the system sensitivity this is taken into account through a pixel efficiency factor, η_{pixel} , which is defined as the fraction of the pixel area to the PSF area.

The spectrometer, and in particular its image slicer, is used over a large wavelength range. The (spatial) pixel scale is a compromise between resolution at short wavelengths and observing efficiency (mapped area) at long wavelengths. Full spatial sampling will require a fine raster with the satellite, for spectral line maps with full spatial resolution. For the sensitivity calculation this is neglected as the line flux will always be collected with the filled detector array. Therefore, for the plain detection of a line source, one pointing is sufficient. Fully resolved maps will require between 2 and 8 raster pointings, between the long and short wavelength end of the spectrometer range, with correspondingly longer integration time.

The spectral sampling also varies within each grating order; detection to the instantaneous resolution as given by the convolution of the diffraction-limited resolution with the pixel function is the default for the sensitivity estimates.

4.8. System Sensitivity

For the calculation of the system sensitivity we have compiled the efficiency of the optical elements in the detection path in Table 1 for the photometer and the spectrometer channels. Table 2 shows the derived transmission for the different sources of thermal background radiation as well as for the light from the astronomical source.

optical element	efficiency	
	photometry	spectroscopy
Lyot stop	0.9	0.9
filters	0.4	0.4
mirrors	0.85	0.74
slicer diffraction	–	0.85
grating	–	0.65

Table 1. *Efficiency of optical elements adopted for calculating system transmission and background.*

The system NEP has been calculated with the parameters from Tables 1 and 2. Results for photometry and spectroscopy at a few representative wavelengths are listed in Table 3, both referred to the detector and referred to the sky including all losses in the system.

Table 3 gives an overview of the background and the NEPs for the different modes of operation, both referred to the detector and referred to the sky including all losses in the system.

5. SUMMARY OF SCIENTIFIC CAPABILITIES OF PACS

5.1. The Photometer

In photometer mode, PACS has imaging capability in two wavelength bands simultaneously, centered at $\lambda = 110\mu\text{m}$ or $\lambda = 75\mu\text{m}$ and $\lambda = 170\mu\text{m}$, with a resolution of $\lambda/\Delta\lambda \approx 2.3$. The two imaging trains are split by a dichroic beamsplitter, such that the centres of the two fields-of-view coincide on the sky and can be observed simultaneously. Plate scale in each band is adjusted to provide approximately full spatial sampling of the telescope PSF at the nominal wavelength of each channel. The following table summarises the pertinent performance data.

level	T (K)	ϵ	effective transmission		relative bandwidth	
			photometry	spectroscopy	photometry	spectroscopy
telescope	100	0.04	0.31	0.15	1/2.5 / 1/2.2 ^(a)	1/1700
baffle	65	0.01	0.34	0.16	1/2.5 / 1/2.2 ^(a)	1/1700
“15 K” optics	15	0.05	0.34	0.16	1/2.5 / 1/2.2 ^(a)	1/1700
“4 K” optics	5.5	0.15	4 ^(b)	4 ^(b)	1/1.5	1/1.5

(a) Values for the photometry modes from 60 – 90 / 90 – 130 μm and 130 – 210 μm , respectively. (b) The formal transmission of 4 takes into account the acceptance solid angle of the light cones which differs from the beam solid angle.

Table 2. Parameters used for estimating the thermal background reaching the detectors. Effective transmission defines the fraction of light originating from the respective level that reaches the detector.

λ (μm)	R	Telescope efficiency	$\eta_{\text{pixel}}^{(a)}$	Background (W)	BLIP NEP ^(b) (W Hz ^{-1/2})	Coupling ^(c) correction	System NEP (W Hz ^{-1/2})
60	1700	0.55	1	4.3×10^{-14}	4.4×10^{-17}	28	1.2×10^{-15}
90	1700	0.69	1	2.6×10^{-14}	2.8×10^{-17}	22	6.2×10^{-16}
130	1700	0.74	0.64	1.3×10^{-14}	1.6×10^{-17}	25	4.3×10^{-16}
180	1700	0.77	0.34	6.8×10^{-15}	1.0×10^{-17}	34	3.8×10^{-16}
60 – 90	2.5	0.64	0.14	8.2×10^{-12}	5.4×10^{-16}	30	1.6×10^{-14}
90 – 130	2.5	0.73	0.12	4.4×10^{-12}	3.3×10^{-16}	29	9.4×10^{-15}
130 – 210	2.5	0.77	0.20	7.9×10^{-12}	3.5×10^{-16}	21	7.4×10^{-15}

(a) The plate scale for the photoconductive arrays was chosen to achieve approximately full beam sampling in photometry mode, and as a compromise between resolution and efficiency in spectroscopy mode. The light from a point source is therefore distributed over several pixels which is represented by the pixel efficiency $\eta_{\text{pixel}} = \Omega_{\text{pixel}} \times (1.48 \times \lambda/D)^{-2}$. However, as the telescope will be diffraction limited only at $\lambda > 100\mu\text{m}$, we have set $\lambda = 90\mu\text{m}$ for the calculation of pixel efficiencies at the shortest wavelengths

(b) The BLIP NEP is defined as the optical power incident onto the detector that produces a signal equal to the r.m.s. noise measured under the quoted background conditions. The quantum efficiency and generation/recombination noise are taken into account, but otherwise the detector is assumed to be noise free. The detector quantum efficiency was assumed to be 30%. The detector NEP, defined as the optical power equivalent to the intrinsic noise of the combination of detector and readout electronics under dark condition, is expected to be $\sim 5 \times 10^{-18} \text{ W Hz}^{-1/2}$.

(c) The coupling factor is defined as $(\tau_{\text{cold}} \times \eta_{\text{chop}} \times \eta_{\text{tel}} \times \eta_{\text{pixel}}^{1/2})^{-1}$ where τ_{cold} is the transmission of the instrument as quoted above, η_{chop} is the chopping efficiency (0.45), and η_{tel} is the telescope efficiency as listed in the table. The factor $\eta_{\text{pixel}}^{1/2}$ takes into account that, for the photoconductive array, several pixels have to be coadded to recover the light from a point source. The system NEP is obtained by multiplying the geometric sum of the NEPs (background and detector) with the coupling factor.

Table 3. Background and system noise levels in spectroscopy and photometry modes.

5.2. The Spectrometer

The grating spectrometer has a fixed pixel size of 9.4", determined by the image slicer. The FOV of 5 × 5 pixels can be observed with either the long- λ (110 – 210 μm) array or the short- λ (60 – 110 μm) array. The working band and detector array are selected by fixed dichroic and bandpass metal mesh filters (switchable to select the desired grating order in the case of the short- λ band), whereas the observing wavelength is tuned by tilting the grating. Spectra covering $\sim 2000\text{km/s}$ around the selected spectral line are obtained simultaneously for all 25 spatial pixels. A summary of the important operating characteristics of the spectrometer is shown in Table 5.

5.3. Comparison with Other Missions

In Table 6 average numbers for the sensitivity of PACS over its wavelength range are compared with those of similar, existing or planned instruments on other spaceborne or airborne platforms.

Even if we neglect the advantage of FIRST in terms of angular resolution, it is obvious that for point source detection PACS will have better limiting sensitivity than any other mission in the FIR in the foreseeable future.

Pixel size	3.4''	6.8''
FOV (16 × 25 pixel)	55'' × 85''	109'' × 170''
Wavelength range	60 – 90/90 – 130 μm	130 – 210 μm
Point source detection limit (5 σ, 1 hour)	6.6/5.6 (4.7/4.0)* mJy	6.0 (4.2)* mJy

*) with on-array chopping

Table 4. *PACS Photometer Mode Specifications*

Pixel size	9.4''	
FOV (5 × 5 pixel)	47'' × 47''	
Wavelength range	57 μm–210 μm	
Resolution ($c\Delta\lambda/\lambda$)	100 – 250 km/s *	
Instantaneous spectral coverage	1300 – 3000 km/s *	
Point source detection limit (5 σ, 1 hour)	λ = 60 μm	$7.8(5.5)** \times 10^{-18} \text{W/m}^2$
	λ = 90 μm	$4.0(2.8)** \times 10^{-18} \text{W/m}^2$
	λ = 130 μm	$2.8(2.0)** \times 10^{-18} \text{W/m}^2$
	λ = 180 μm	$2.5(1.8)** \times 10^{-18} \text{W/m}^2$

*) varies with wavelength

**) with on-array chopping

Table 5. *PACS Spectrometer Mode Specifications*

Mode	FIRST-PACS	SOFIA	ISO	SIRTF
Photometry	6 (4)* mJy	50 mJy	15...100 mJy**	8...55 mJy**
Spectroscopy	$3 \times 10^{-18} \text{W/m}^2$	$2.5 \times 10^{-17} \text{W/m}^2$	$4.5 \times 10^{-17} \text{W/m}^2$	—

*) with on-array chopping

**) confusion limited

Table 6. *Sensitivity of FIRST-PACS (point source detection, 5 σ, 1 hour) compared to present and planned platforms.*

In its medium-resolution line spectroscopy mode it will be unrivaled. For point source photometry, SIRTF will be superior in terms of raw sensitivity, but fall short for deeper surveys due to confusion. For extended sources where the angular resolution of FIRST is not required, SIRTF with its cryogenic telescope will clearly be the instrument of choice and an ideal complement to FIRST.

ACKNOWLEDGMENTS

This paper represents work carried out by the PACS consortium which consists at this time of the following institutes: Max-Planck-Institut für extraterrestrische Physik (MPE; D), Max-Planck-Institut für Astronomie (MPIA; D), Universitätsternwarte Jena (D), Katholieke Universiteit Leuven (KUL; B), Centre Spatial de Liège (CSL; B), Laboratoire d'Astronomie Spatial + Observatoire Marseille (IGRAP; F), Universität Wien + Technische Universität Wien (A), Instituto de Astrofísica de Canarias (IAC; E), Osservatorio Astrofisico di Arcetri (OAA; I), Istituto di Fisica dello Spazio Interplanetario (IFSI; I), Università di Padova (I).

REFERENCES

1. G. Pilbratt in *The Far Infrared and Submillimetre Universe*, A. Wilson, ed., *Proc. ESA Symposium ESA SP-401*, p. 7, 1997.
2. N. D. Whyborn in *The Far Infrared and Submillimetre Universe*, A. Wilson, ed., *Proc. ESA Symposium ESA SP-401*, p. 19, 1997.
3. A. Poglitsch in *The Far Infrared and Submillimetre Universe*, A. Wilson, ed., *Proc. ESA Symposium ESA SP-401*, p. 25, 1997.

4. M. J. Griffin in *The Far Infrared and Submillimetre Universe*, A. Wilson, ed., *Proc. ESA Symposium ESA SP-401*, p. 31, 1997.
5. G. Pilbratt in *Space Telescopes and Instruments V*, P. Bely and J. Breckinridge, eds., *Proc. SPIE 3356*, pp. 452–461, 1998.
6. T. de Graauw et al. in *Advanced Technology MMW, Radio, and Terahertz Telescopes*, T. Phillips, ed., *Proc. SPIE 3357*, pp. 336–347, 1998.
7. A. Poglitsch in *Infrared Astronomical Instrumentation*, A. Fowler, ed., *Proc. SPIE 3354*, pp. 1032–1043, 1998.
8. M. Griffin, L. Vigroux, and B. Swinyard in *Advanced Technology MMW, Radio, and Terahertz Telescopes*, T. Phillips, ed., *Proc. SPIE 3357*, pp. 404–413, 1998.
9. R. Graue and D. Kampf in *UV, Optical, and IR Space Telescopes and Instruments*, J. Breckinridge and P. Jakobsen, eds., *Proc. SPIE 4013*, p. (this volume), 2000.
10. R. Katterloher, D. Engemann, M. Fabricotti, O. Frenzl, L. Hermans, D. Lemke, J. Wolf, E. Czech, E. Haller, N. Haegel, M. Konuma, and G. Pilbratt in *The Far Infrared and Submillimetre Universe*, A. Wilson, ed., *Proc. ESA Symposium ESA SP-401*, p. 393, 1997.
11. J. Wolf, R. Katterloher, D. Lemke, U. Grözinger, L. Hermans, O. Frenzl, D. Engeman, J. Beeman, and M. Fabricotti in *Submillimetre and Far-Infrared Space Instrumentation*, E. J. Rolfe, ed., *Proc. ESA Symposium ESA SP-388*, p. 25, 1996.
12. S. Kraft, O. Frenzl, L. Hermans, R. Katterloher, D. Rosenthal, U. Grözinger, and J. Beeman in *Infrared Spaceborne Remote Sensing VII*, M. Scholl, ed., *Proc. SPIE 3759*, pp. 214–220, 1999.
13. S. Kraft, O. Frenzl, L. Hermans, R. Katterloher, D. Rosenthal, U. Grözinger, and J. Beeman in *UV, Optical, and IR Space Telescopes and Instruments*, J. Breckinridge and P. Jakobsen, eds., *Proc. SPIE 4013*, p. (this volume), 2000.
14. O. Charlier in *UV, Optical, and IR Space Telescopes and Instruments*, J. Breckinridge and P. Jakobsen, eds., *Proc. SPIE 4013*, p. (this volume), 2000.
15. H. Bischof, D. Hoenigmann, and F. Kerschbaum in *UV, Optical, and IR Space Telescopes and Instruments*, J. Breckinridge and P. Jakobsen, eds., *Proc. SPIE 4013*, p. (this volume), 2000.
16. F. Kerschbaum, H. Bischof, D. Hoenigmann, and T. Lebzelter in *UV, Optical, and IR Space Telescopes and Instruments*, J. Breckinridge and P. Jakobsen, eds., *Proc. SPIE 4013*, p. (this volume), 2000.
17. D. Lemke, U. Grözinger, O. Krause, R. Rohloff, and R. Haberland in *Infrared Spaceborne Remote Sensing VII*, M. Scholl and B. Andresen, eds., *Proc. SPIE 3759*, pp. 205–213, 1999.
18. E. Renotte, J. Gillis, C. Jamar, P. Laport, T. Salée, and S. Crehay in *Infrared Spaceborne Remote Sensing VII*, M. Scholl, ed., *Proc. SPIE 3759*, pp. 189–204, 1999.
19. A. Poglitsch, C. Waelkens, and N. Geis in *Infrared Spaceborne Remote Sensing VII*, M. Scholl and B. Andresen, eds., *Proc. SPIE 3759*, pp. 221–233, 1999.
20. N. Hiromoto, T. Itabe, T. Aruga, H. Okuda, H. Matsuhara, H. Shibai, T. Nakagawa, and T. Saito *IR Phys.* **29**, p. 255, 1989.
21. G. J. Stacey, J. W. Beeman, E. E. Haller, N. Geis, A. Poglitsch, and M. Rumitz *Int J. IR & Millimeter Waves.* **13**, p. 1689, 1992.